


Article

Metal-Organic Framework vs. Coordination Polymer—Influence of the Lanthanide on the Nature of the Heteroleptic Anilate/Terephthalate 3D Network

Mariangela Oggianu ^{1,2}, Fabio Manna ^{1,3}, Suchithra Ashoka Sahadevan ^{1,3}, Narcis Avarvari ³ , Alexandre Abhervé ^{3,*} and Maria Laura Mercuri ^{1,2,*}

- ¹ Dipartimento di Scienze Chimiche e Geologiche, Università degli Studi di Cagliari, I-09042 Monserrato, Cagliari, Italy; mari.oggianu@gmail.com (M.O.); fmanna@etud.univ-angers.fr (F.M.); suchithraiserk@gmail.com (S.A.S.)
- ² INSTM, Cagliari Unit, Via Giuseppe Giusti, 9, 50121 Firenze, Italy
- ³ Univ Angers, CNRS, MOLTECH-Anjou, SFR MATRIX, F-49000 Angers, France; narcis.avarvari@univ-angers.fr
- * Correspondence: alexandre.abherve@univ-angers.fr (A.A.); mercuri@unica.it (M.L.M.)

Abstract: Metal-organic frameworks (MOFs), whose definition has been regularly debated, are a sub-class of coordination polymers (CPs) which may feature both an overall 3D architecture and some degree of porosity. In this context, MOFs based on lanthanides (Ln-MOFs) could find many applications due to the combination of sorption properties and magnetic/luminescent behaviors. Here we report rare examples of 3D Ln-CPs based on anilate linkers, obtained under solvothermal conditions using a heteroleptic strategy. The three compounds of formula $[\text{Yb}_2(\mu\text{-ClCNAn})_2(\mu\text{-F}_4\text{BDC})(\text{H}_2\text{O})_4] \cdot (\text{H}_2\text{O})_3$ (**1**), $[\text{Er}_2(\mu\text{-ClCNAn})_2(\mu\text{-F}_4\text{BDC})(\text{H}_2\text{O})_4] \cdot (\text{H}_2\text{O})_4$ (**2**) and $[\text{Eu}_2(\mu\text{-ClCNAn})_2(\mu\text{-F}_4\text{BDC})(\text{H}_2\text{O})_6]$ (**3**) have been characterized by single-crystal X-ray diffraction, thermogravimetric analysis, and optical measurements. Structural characterization revealed that compounds **1** and **2** present an interesting MOF architecture with extended rectangular cavities which are only filled with water molecules. On the other hand, compound **3** shows a much more complex topology with no apparent cavities. We discuss here the origins of such differences and highlight the crucial role of the Ln(III) ion nature for the topology of the CP. Compounds **1** and **2** now offer a playground to investigate the possible synergy between gas/solvent sorption and magnetic/luminescent properties of Ln-MOFs.

Keywords: metal-organic framework; lanthanides; chlorocyananilate; tetrafluoroterephthalate



Citation: Oggianu, M.; Manna, F.; Ashoka Sahadevan, S.; Avarvari, N.; Abhervé, A.; Mercuri, M.L. Metal-Organic Framework vs. Coordination Polymer—Influence of the Lanthanide on the Nature of the Heteroleptic Anilate/Terephthalate 3D Network. *Crystals* **2022**, *12*, 763. <https://doi.org/10.3390/cryst12060763>

Academic Editor: Younes Hanifehpour

Received: 9 May 2022
Accepted: 25 May 2022
Published: 26 May 2022

Publisher's Note: MDPI stays neutral with regard to jurisdictional claims in published maps and institutional affiliations.

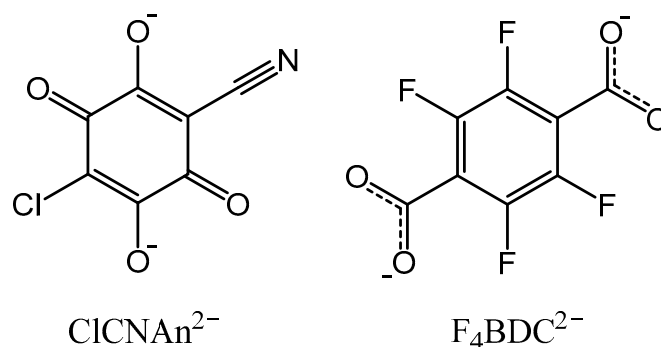


Copyright: © 2022 by the authors. Licensee MDPI, Basel, Switzerland. This article is an open access article distributed under the terms and conditions of the Creative Commons Attribution (CC BY) license (<https://creativecommons.org/licenses/by/4.0/>).

1. Introduction

Coordination polymers (CPs) and metal-organic frameworks (MOFs) are important classes of molecular materials in solid-state and coordination chemistry. However, if the prime definition of a CP was the non-molecular assembly of metal centers through organic linkers by covalent and/or ionic bonds, the CPs/MOFs terminology remained confusing for decades [1]. Even though it was widely accepted that MOFs are a sub-class of CPs [2], the discrimination criteria for MOFs was unclear. From the survey proposed by Öhrström et al. about the definition of a MOF (mostly described as “a network with frames”) [1] as well as the definition given by James (structures “which exhibit porosity”) [3], and based on MOFs properties that are often associated with gas sorption, it seems now approved that a MOF should exhibit a 3D structure with some degree of porosity. Among them, CPs or MOFs based on rare earth metals, especially lanthanide(III) ions (hereafter called Ln-CPs or Ln-MOFs), were especially investigated for magnetic [4] and/or luminescence properties [5–7], but also adsorption [8], sensing properties [9,10], and more recently circularly polarized luminescence [11]. The more flexible coordination numbers and geometries of Ln(III) ions compared to transition metal ions make the prediction of Ln-CPs architectures challenging. Crystal structures topologies and dimensionalities can indeed be

affected by synthetic conditions, the presence of coordinated solvent molecules [12], and the choice of the organic linker [13], but also by the nature of the Ln(III) ion [14]. Most of the ligands used are carboxylates derivatives due to their hard base behavior [2]. Among them, oxalate [15], succinate [16] and some other aliphatic linkers were used [17], but most of the reported examples contain aromatic linkers such as squarate [18,19], 1,4-benzenedicarboxylate (usually called terephthalate) [20], 1,3,5-benzene-tricarboxylate [21] or more extended π -conjugated linkers [22,23], and more recently imidazole [24–26], pyridine [27] or pyrimidine-based bridging ligands [28]. Alternatively, derivatives of 2,5-dihydroxy-1,4-benzoquinone, usually called anilates, have been extensively used in the last decade to prepare CPs with either transition metal ions [29,30] or lanthanides [31]. The choice of the anilate linker could afford interesting magnetic properties due to the presence of magnetic exchange interactions through the bis-bidentate ligand and the redox ability of the anilate. On the other hand, the good antenna effect of the anilate linkers has shown to be efficient especially for near-infrared (NIR) emitting Ln(III) ions [32]. Most examples of Ln(III)-anilate compounds previously reported are 2D coordination polymers [33]. Indeed, while several examples of 3D coordination polymers based on transition metal ions and anilate linkers have been reported [34–36], only three publications have described 3D Ln(III)-anilate compounds [37–39]. However in 2D CPs, the structural versatility was already observed depending either on the nature of the Ln(III) ion or the choice of the solvent, ranging from (4,3) topology with square cavities to (6,3) topology with either strongly distorted rectangular cavities or more regular hexagonal cavities [40]. In order to promote higher dimensionalities of the extended network, one strategy consists in using multiple linkers and thus create additional connections between metal centers. A representative example was reported by Wang et al. with the 3D CP of formula $[\text{Ln}(\text{tpbz})(\text{tdc})]$ (Ln = Sm, Eu, Tb) obtained by the use of both 4-(2,2':6',2''-terpyridin-4'-yl)benzoate (tpbz) and 2,5-thiophenedicarboxylate (tdc) [13]. One less conventional example was reported by the team of Wu, where hydrolysis of DMF could induce the formation of formate (fa) ligands followed by the crystallization of Ln-CPs of formula $[\text{Ln}(\text{tpa})(\text{fa})]$ (Ln = Eu, Gd, Tb; tpa = terephthalate). In these series of compounds, 2D Ln-formate layers were further connected by tpa linkers to form an overall 3D network [41]. As part of our research endeavor on anilate Ln-CPs, we applied herein the multiple linkers strategy, hereafter called heteroleptic strategy, in order to afford 3D Ln-CPs based on the anilate ligands. We thus selected the 3-chloro-6-cyano-2,5-dihydroxy-1,4-benzoquinone (chlorocyananilate, ClCNAn^{2-}) and 2,3,5,6-tetrafluoroterephthalate ($\text{F}_4\text{BDC}^{2-}$, Scheme 1) [42,43] bridging ligands since the use of these two linkers already allowed some of us to obtain heteroleptic 2D Ln-CPs [44,45]. In this work, we have been able to crystallize in a highly reproducible manner, under solvothermal conditions, the 3D compounds of formula $[\text{Yb}_2(\mu\text{-ClCNAn})_2(\mu\text{-F}_4\text{BDC})(\text{H}_2\text{O})_4] \cdot (\text{H}_2\text{O})_3$ (**1**), $[\text{Er}_2(\mu\text{-ClCNAn})_2(\mu\text{-F}_4\text{BDC})(\text{H}_2\text{O})_4] \cdot (\text{H}_2\text{O})_4$ (**2**) and $[\text{Eu}_2(\mu\text{-ClCNAn})_2(\mu\text{-F}_4\text{BDC})(\text{H}_2\text{O})_6]$ (**3**). Crystal structures determinations reveal that in compounds **1** and **2** the 3D network is made by six-membered rings with regular rectangular shape and presence of large extended cavities, therefore **1** and **2** can be described as Ln-MOFs, while compound **3** presents a dense and more complex architecture with no apparent voids, highlighting the influence of the Ln(III) on the nature of the Ln-CP.



Scheme 1. Structures of the bridging ligands used in this work.

2. Materials and Methods

2.1. Materials

Reagents were purchased from Zentek (TCI) and used without further purification. KHCICNA n was synthesized as previously reported [46].

2.2. Synthesis

Compounds **1**, **2**, and **3** were synthesized via hydrothermal approach. A 80 mL Teflon-lined stainless-steel autoclave reactor with a mixture of Ln(NO₃)₃ · xH₂O (Ln^{III} = Yb^{III}, Er^{III} and Eu^{III}) (0.3 mmol), KHCICNA n (0.15 mmol), H₂F₄BDC (0.15 mmol), NaOH (0.45 mmol) and water (40 mL) was heated at 100 °C for 48 h. After cooling to room temperature, red crystals suitable for X-ray diffraction analysis were obtained.

2.3. X-ray Crystallography

Single crystals of compounds **1**, **2**, and **3** were mounted on glass fiber loops using a viscous hydrocarbon oil to coat the crystal and then transferred directly to the cold nitrogen stream. Data collection were performed on an Agilent Supernova with Cu-K_α (λ = 1.54184 Å). The structures were solved by direct methods with the SIR97 program and refined all F² values with the SHELXL-2016/4 program using the WinGX graphical user interface. All non-hydrogen atoms were refined anisotropically. All hydrogen atoms were placed in calculated positions and refined isotropically with a riding model. A summary of the crystallographic data and the structure refinement is given in Table S1. CCDC 2170833-2170835 contain the supplementary crystallographic data for the paper. These data can be obtained free of charge from The Cambridge Crystallographic Data Centre. Powder X-ray diffraction was performed on a D8 Advance diffractometer from Bruker.

2.4. Thermogravimetric Analysis (TGA)

A TGA Q500 from TA Instruments was used for TGA under a nitrogen flow of 40 mL·min⁻¹ at atmospheric pressure. A total of 10 mg of **1**, 4 mg of **2** and 8 mg of **3** was placed on a platinum crucible, and measurements were performed in the temperature range 25–1000 °C at a heating rate of 20 °C min⁻¹.

2.5. Vibrational and Optical Spectroscopy Measurements

Fourier-transform infrared spectroscopy (FT-IR) was performed on KBr pellets and collected with a Bruker Equinox 55 FT-IR spectrometer. Reflectance spectroscopy measurements were performed under sample direct illumination in a dual-beam spectrophotometer (Agilent Technologies Cary 5000 UV-Vis-NIR) equipped with a diffuse reflectance integration sphere.

3. Results and Discussions

3.1. Synthesis

Compounds **1**, **2**, and **3** were obtained by combining Yb^{III}, Er^{III} and Eu^{III} salts with both organic linkers ClCNAn²⁻ and F₄BDC²⁻ under hydrothermal conditions. This method allowed to directly isolate the 3D coordination polymers as single crystals suitable for X-ray analysis. The purity of the polycrystalline samples was confirmed by FT-IR (Figure S1) and powder X-ray diffraction (Figures S2–S4). It should be noted that in our previous studies [44,45], one-pot room-temperature synthesis or layering techniques were used using the same precursor reagents and resulted in 2D coordination polymers. It thus highlights the influence of solvothermal conditions on the crystallization of 3D structures.

3.2. Crystal Structures of [Yb₂(μ-ClCNAn)₂(μ-F₄BDC)(H₂O)₄](H₂O)₃ (**1**) and [Er₂(μ-ClCNAn)₂(μ-F₄BDC)(H₂O)₄](H₂O)₄ (**2**)

Compounds **1** and **2** crystallized in the triclinic space group *P*-1 and are isostructural. The asymmetric units contain one independent metal ion, two half chlorocyananilate (ClCNAn²⁻) ligands, one half tetrafluoroterephthalate (F₄BDC²⁻) ligand and two coordinated water molecules (Figure 1). The Yb or Er metal ion is linked to four O atoms from ClCNAn²⁻ bridging ligands, two O atoms from F₄BDC²⁻ and two O atoms from water molecules. Therefore, the metal ion is eight-coordinated within a strongly distorted trigonal prism geometry (C_{2v} local symmetry) as shown by CShM values of 1.151 and 1.174 for Yb and Er respectively (Figure S5) [47]. The ClCNAn²⁻ ligand coordinates two metal ions in a bis-bidentate mode, while the F₄BDC²⁻ ligand coordinates four metal ions in a tetradentate mode. As a consequence of this coordination mode, one-dimensional (1D) chains of Ln(III) connected by carboxylate groups are formed along the crystallographic *a* axis and show short metal-metal distances (Yb⋯Yb distance of 5.07 Å, Er⋯Er distance of 5.11 Å). These chains are separated by the anilate and F₄BDC²⁻ ligands with shortest distances between metal ions of 8.64 and 9.69 Å for Yb and 8.68 and 9.69 for Er (Figure S6).

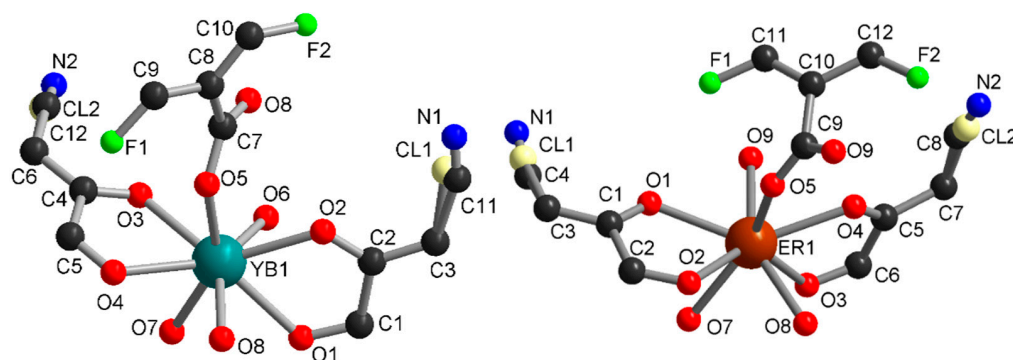


Figure 1. Asymmetric unit in **1** (left) and **2** (right).

1 can also be described as two-dimensional (2D) metal-anilate layers running along the (0-11) lattice plane and connected together by the F₄BDC²⁻ ligands. Indeed, the two ClCNAn²⁻ ligands are *trans* on the polyhedron, leading to an Ln(III)-ClCNAn²⁻ 1D chain (Figure 2). These 1D chains are connected to each other by the first bidentate carboxylate group from the F₄BDC²⁻ ligand to form 2D layers. Finally, with the coordination of the second carboxylate group, the F₄BDC²⁻ ligand is able to bridge the layers and form the 3D architecture (Figure 2 and Figure S7). Along the *a* axis, extended rectangular cavities are formed by the 1D anilate-based chains connected together by F₄BDC²⁻ spacers affording a 3D MOF (Figure 3). The accessible voids are calculated at 128 Å³ per cell (and per formula unit) in **1** and 153 Å³ in **2**. These cavities are filled with water solvent molecules (three per formula unit in **1** and four per formula unit in **2** according to the SQUEEZE procedure).

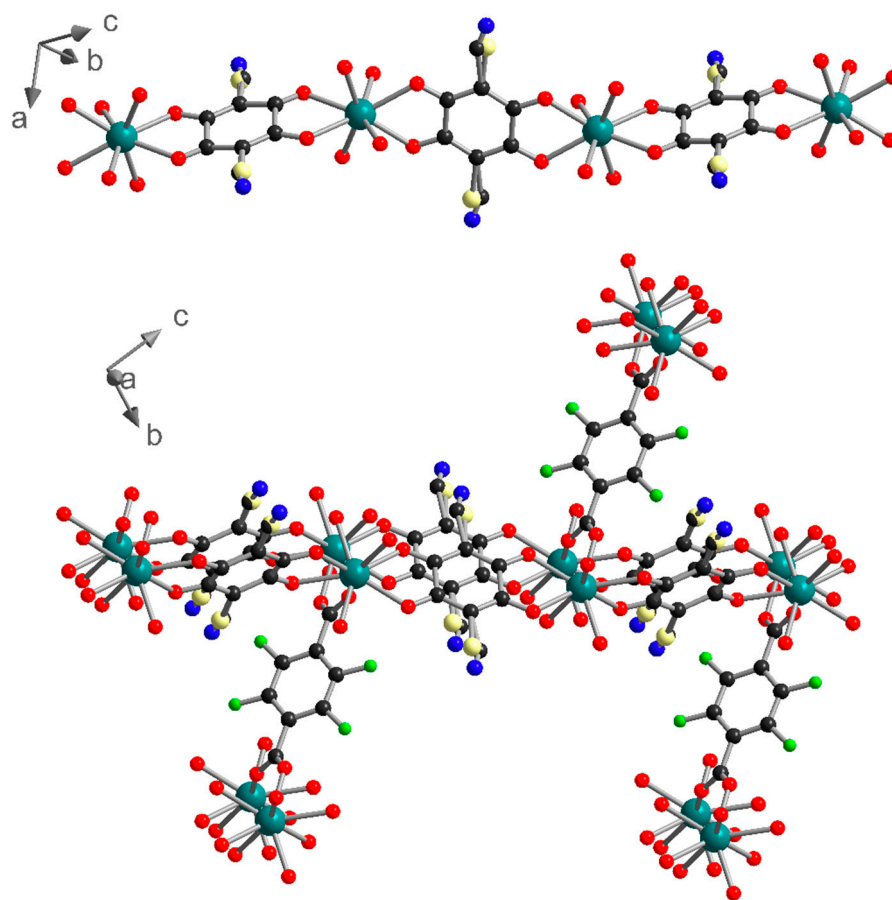


Figure 2. 1D chain of Yb-CICNAn²⁻ (**top**) and 3D network made by the connection of 1D chains with F₄BDC²⁻ ligands (**bottom**) in **1**. Color code: C (black), O (red), N (blue), F (green), Cl (light yellow), Yb (teal).

3.3. Crystal Structure of [Eu₂(μ-CICNAn)₂(μ-F₄BDC)(H₂O)₆] (**3**)

Compound **3** crystallized in the monoclinic space group *I2/a*. The asymmetric unit contains one independent metal ion, two half CICNAn²⁻ ligands, one-half F₄BDC²⁻ ligand and three water molecules (Figure 4). The Eu metal ion is linked to four O atoms from CICNAn²⁻, two O atoms from F₄BDC²⁻ and three O atoms from water molecules. Therefore, the Eu metal ion is nine-coordinated within a strongly distorted tricapped trigonal prism geometry (*D*_{3h} local symmetry) toward a capped square antiprism (*C*_{4v}), with CShM values of 0.948 and 1.074 respectively. The metal ion is surrounded by two CICNAn²⁻ ligands on opposite sides of the polyhedron and two adjacent F₄BDC²⁻ ligands, while the three water molecules are organized in a *fac* manner (Figure S5). The bridging ligands present the same coordination mode as in **1** and **2** (bis-bidentate and tetradentate modes for CICNAn²⁻ and F₄BDC²⁻, respectively). Therefore, the crystal structure can also be described as Eu-CICNAn²⁻ 1D chains connected to each other by F₄BDC²⁻ ligands leading to a 3D network (Figures 5 and 6). The carboxylate bridges lead to the shortest Eu⋯Eu distances of 5.56 Å, while the CICNAn²⁻ linkers lead to distances between metal ions of 8.76 and 8.90 Å. In addition, a short Eu⋯Eu distance of 6.30 Å can be observed between two non-bridged metal ions (Figure S8).

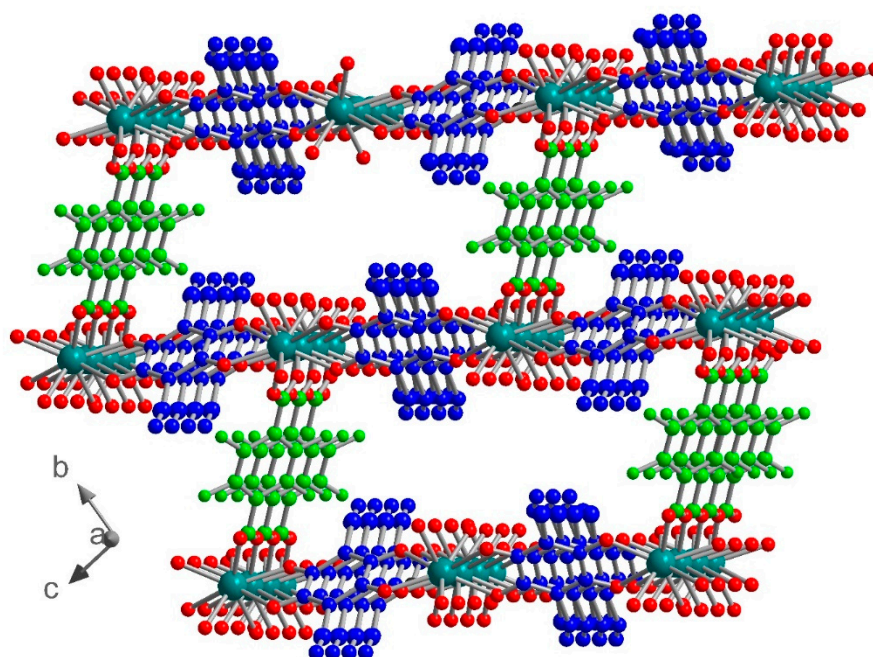


Figure 3. View of the crystal structure in **1** showing the rectangular cavities along the *a* axis. CICNAn^{2-} and $\text{F}_4\text{BDC}^{2-}$ are highlighted in blue and green, respectively.

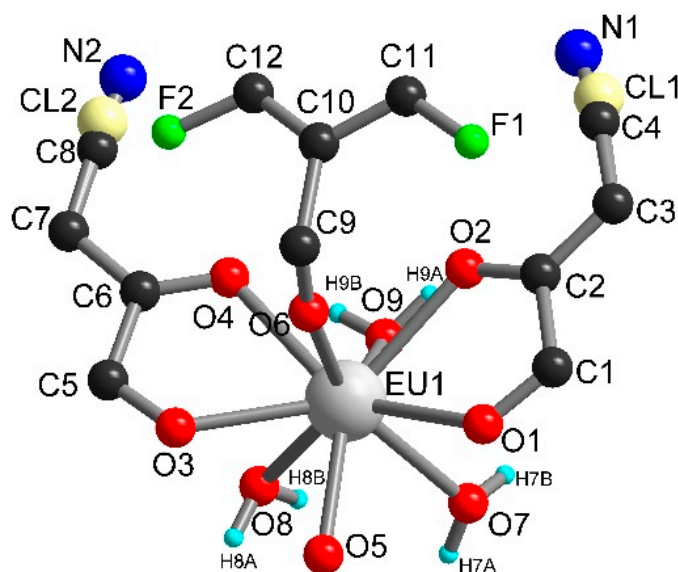


Figure 4. Asymmetric unit in **3**.

Although the three crystal structures share many features such as the metal to ligands stoichiometry ($\text{Ln}/\text{CICNAn}^{2-}/\text{F}_4\text{BDC}^{2-}$ ratio of 2/2/1) and the coordination mode of the ligands, the resulting 3D networks present very different topologies. This first originates from the size and coordination number of the metal ion (eight-coordinated for Yb/Er, nine-coordinated for Eu). As a result, the two adjacent $\text{F}_4\text{BDC}^{2-}$ ligands from the same polyhedron lie parallel to each other in **1** and **2**, while they are oriented in opposite directions in the Eu compound (Figures 7 and S5). Moreover, in **1** and **2** linear Ln(III)-carboxylate chains run along the *a* direction, while in **3** the Ln(III) ions are not eclipsed along the 1D chains (Figure 7). Therefore, in **1** and **2** all Ln(III)-anilate 1D chains lie in the (0-11) lattice plane and the $\text{F}_4\text{BDC}^{2-}$ in the (011) plane, leading to the formation of extended rectangular cavities along the *a* axis which are filled with water solvent molecules (Figure S9). In addi-

tion, in **3** one of the two independent half-anilate ligands presents a distortion which can be highlighted by a non-negligible dihedral angle of around 11° between the plane made by the C and O atoms from the ligand and the plane made by the Ln(III) metal center and coordinated O atoms (Figure S10). On the other hand, the second half-anilate ligand is almost coplanar to the Ln(III) metal centers. This results in the strong curvature of the extended Ln(III)-anilate layer. Consequently, **3** is a coordination polymer showing a more complex topology with the absence of apparent cavities and crystallization solvent molecules.

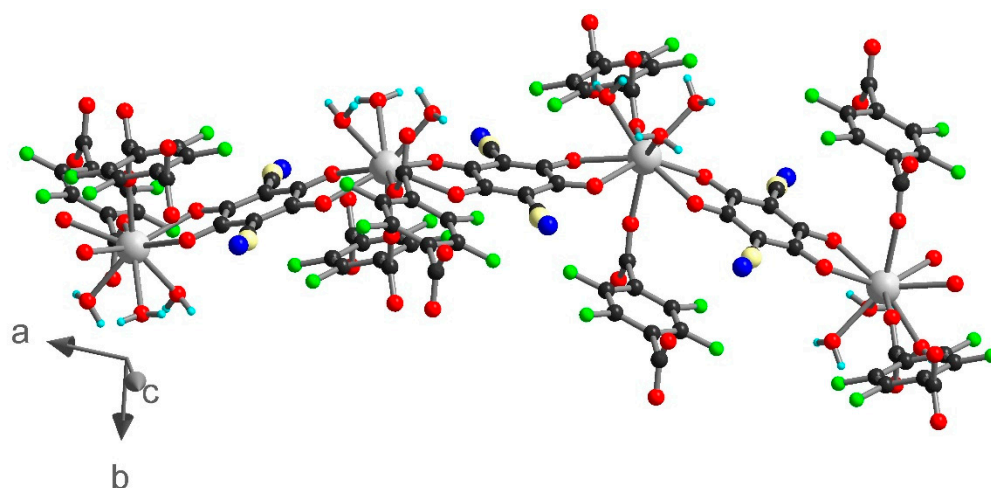


Figure 5. 1D chain of Eu-CiCNAn^{2-} connected by $\text{F}_4\text{BDC}^{2-}$ ligands in **3**. Color code: C (black), H (cyan), O (red), N (blue), F (green), Cl (light yellow), Eu (grey).

3.4. Thermogravimetric Analysis (TGA)

TGA was performed on polycrystalline samples of **1**, **2**, and **3** (Figure S11). The main difference between both compounds is the first loss of weight (about 4 and 6%) in **1** and **2**, corresponding to the loss of between three and four water solvent molecules, in agreement with the number of water molecules calculated in the cavities of the MOF structures. In **3**, such loss was not observed below 100°C . Between 100 and 300°C , **1** and **2** show an additional loss of about 6–7% of weight, which may correspond to the loss of four coordinated water molecules. However, in **3**, the 5% weight loss may correspond to only three over the six coordinated water molecules. Above 375°C , the three compounds present an important weight loss, although this was more gradual in **1** and **2** (which is attributed to the 3D networks collapse).

3.5. Optical Characterization

The diffuse reflectance (DR) spectra spanning through the UV-Vis-NIR spectral range show evidence of both CiCNAn^{2-} ligand and Yb/Er presence (Figure 8). The absorption onset of CiCNAn^{2-} is clearly visible below 650 nm in all compounds. At longer wavelengths, the spectra are dominated by Yb(III) and Er(III) absorption transitions (979 nm for Yb(III), 1510 , 971 and 790 nm for Er(III)) [44,45]. On the other hand, absorption transitions associated to Eu(III) are not visible due to the overlap with those of CiCNAn^{2-} organic linker. The band at $\sim 1450\text{ nm}$ in **1** and **2** was assigned to water absorption (this vibration is a combination of symmetrical and antisymmetrical stretchings of the coordinated water molecule) [45,48].

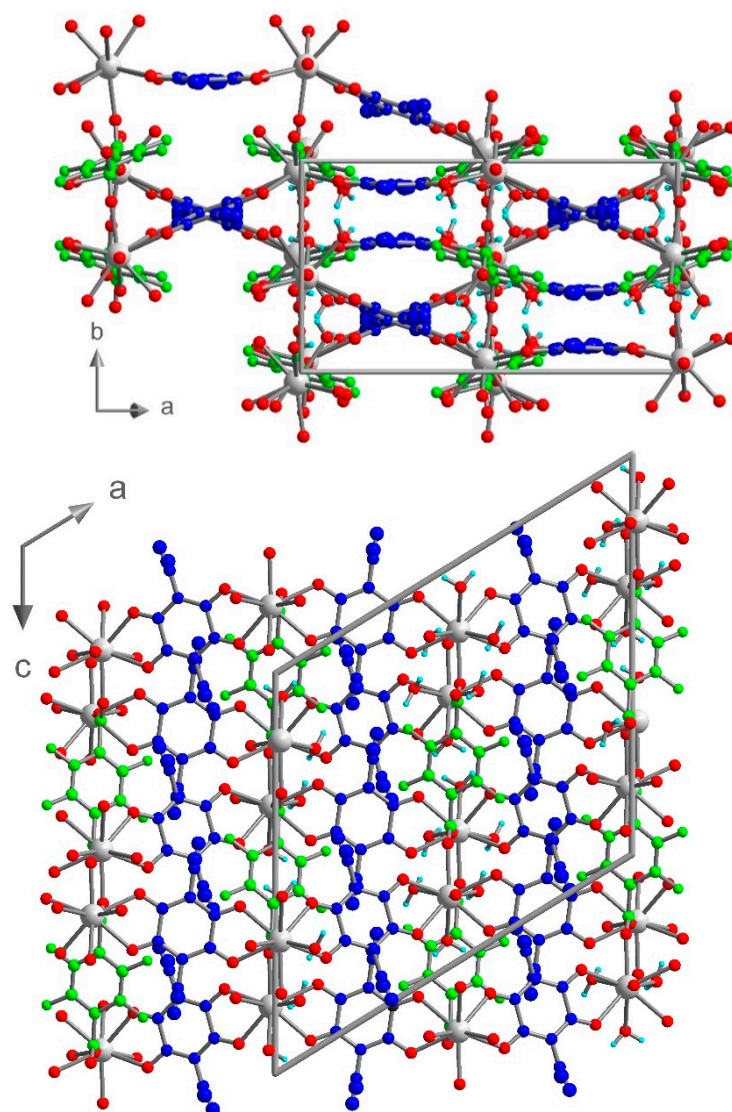


Figure 6. View of the crystal structure of **3** in the *ab* plane (**top**) and in the *ac* plane (**bottom**). CICNAn^{2-} and $\text{F}_4\text{BDC}^{2-}$ are highlighted in blue and green respectively.

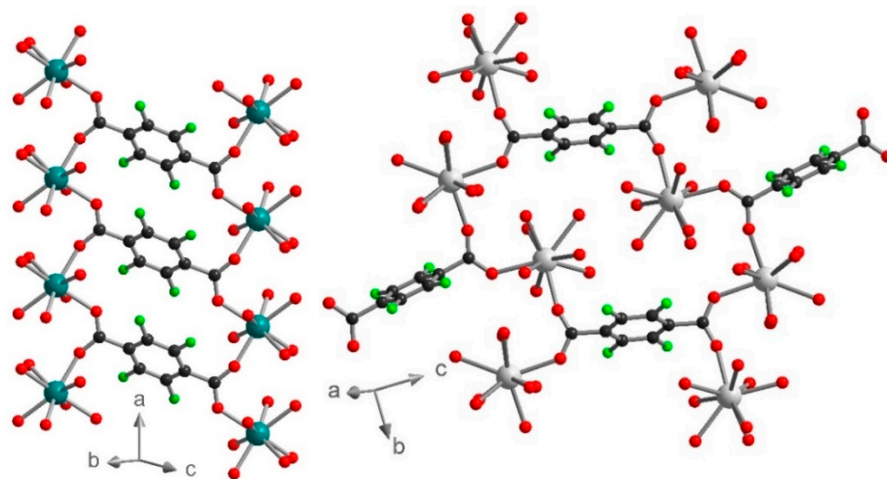


Figure 7. Coordination mode and orientation of the $\text{F}_4\text{BDC}^{2-}$ ligands in **1** (**left**) and **3** (**right**). Color code: C (black), O (red), F (green), Yb (teal), Eu (grey).

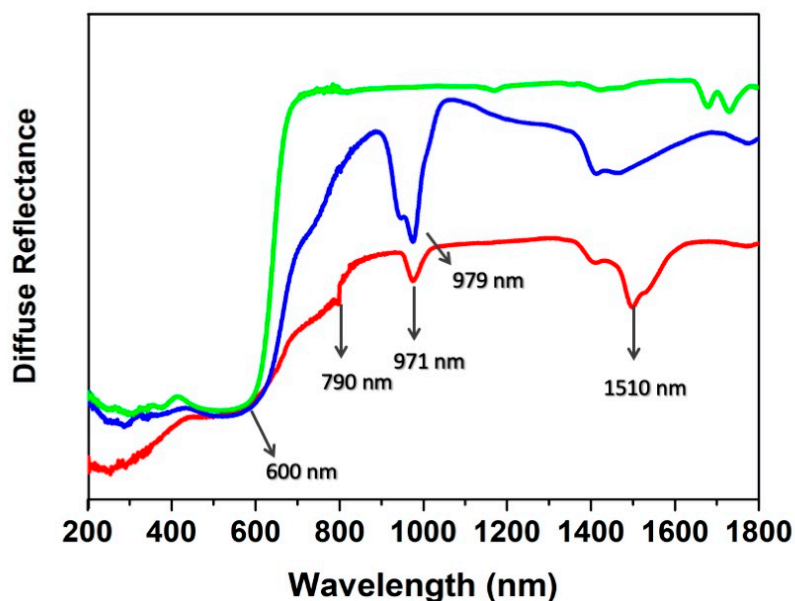


Figure 8. Diffuse reflectance spectra of 1 (blue line), 2 (red line) and 3 (green line).

4. Conclusions

Using the heteroleptic strategy, we have been able to prepare and structurally characterize 3D coordination polymers based on Ln(III) ions and anilate/terephthalate bridging ligands. Notably, the solvothermal synthetic protocol herein optimized seems to play a role in determining the higher dimensionality (3D) and MOF architectures of the materials, especially when compared with room-temperature one-pot synthesis, which has afforded 2D coordination polymers with the same bridging ligands and NIR-emitting lanthanides [44,45]. The resulting crystal structure is strongly affected by the nature of the Ln(III) ion. With Yb(III) and Er(III), the 3D architecture in 1 and 2 is based on Ln(III)-anilate 1D chains connected along the two adjacent directions by tetradentate terephthalate linkers and eclipsed along the *a* direction leading to an Ln-MOF with extended rectangular cavities and structural porosity. On the other hand, with the use of Eu, the 3D architecture of 3 is more complex due to the curvature observed in the Ln(III)-anilate 1D chains and of the many distinct positions of the terephthalate linkers around those chains. TGA confirmed the stability of the 3D network up to 375 °C and the presence of solvent water molecules in the MOF structure of 2. Diffuse reflectance studies have shown to be a valuable probe to identify the presence of water in the inner coordination sphere of the Ln(III) ion [48]. In the progress of this work, the adsorption and luminescence properties of Yb(III), Er(III) and Nd(III) Ln-MOFs will be studied for application in sensing or molecular recognition in the NIR region. On the other hand, we are currently exploiting the use of different Ln(III) ions, as Dy(III) and Tb(III), to provide 3D networks with interesting magnetic properties such as ferro/ferrimagnetism and/or single-molecule-magnet behavior.

Supplementary Materials: The following supporting information can be downloaded at: <https://www.mdpi.com/article/10.3390/cryst12060763/s1>. Table S1: Crystallographic data for 1–3; Figure S1: FT-IR spectra of KHCNAn, H₂F₄BDC, 1, 2 and 3 in the 2000–700 cm^{−1} region; Figures S2–S4: Simulated (black) and experimental (blue) X-ray powder patterns of 1 (S2), 2 (S3) and 3 (S4); Figure S5: Coordination environment of the metal ion in 1 and 3; Figure S6: View of the crystal structures of 1 and 2 in the *ac* plane highlighting the shortest Ln(III)···Ln(III) distances; Figure S7: Views of the extended structure in 1; Figure S8: View of the crystal structure of 3 highlighting the shortest Eu···Eu distances; Figure S9: View of the crystal structure of 1 highlighting the (011) and (0-11) lattice planes; Figure S10: View of the Eu-anilate 1D chain of 3 highlighting the plane of the ligand (in blue) and the plane made by the Ln metal centre and the two coordinated O atoms (in red); Figure S11: TGA of compounds 1, 2 and 3.

Author Contributions: Conceptualization, N.A., A.A. and M.L.M.; synthesis, M.O., F.M. and S.A.S.; structural characterization, F.M. and A.A.; optical characterization, M.O.; writing, A.A. and M.L.M.; review and editing, all authors. All authors have read and agreed to the published version of the manuscript.

Funding: This research was funded in Italy by the Fondazione di Sardegna, Convenzione triennale tra la Fondazione di Sardegna e gli Atenei Sardi, Regione Sardegna, L.R. 7/2007 annualità 2018, through Projects F74I19000940007 and F74I19000920007 for the post-doctoral fellowship of MO. MIUR (Ministry of Education, University, Research) UNICA-UNISS Consortium PhD Course on Chemical Sciences and Technologies is also acknowledged for the PhD grant of FM. CESA (Centro d' Eccellenza per la Sostenibilità Ambientale, accordo di programma RAS-UNICA-IGEA-AUSI, project number E58C16000080003) is acknowledged for the PhD grant of MO. The work in France was supported by the CNRS, the University of Angers, and the RFI LUMOMAT network (ASCO MMM project).

Data Availability Statement: The data presented in this study are available on request from the corresponding authors.

Conflicts of Interest: The authors declare no conflict of interest.

References

1. Batten, S.R.; Champness, N.R.; Chen, X.-M.; Garcia-Martinez, J.; Kitagawa, S.; Öhrström, L.; O'Keeffe, M.; Pail Suh, M.; Reedijk, J. Coordination polymers, metal-organic frameworks and the need for terminology guidelines. *CrystEngComm* **2012**, *14*, 3001–3004. [[CrossRef](#)]
2. De Lill, D.T.; Cahill, C.L. coordination polymers of the lanthanide elements: A structural survey. *Progr. Inorg. Chem.* **2007**, *55*, 143–204.
3. James, S.L. Metal-organic frameworks. *Chem. Soc. Rev.* **2003**, *32*, 276–288. [[CrossRef](#)]
4. Saines, P.J.; Bristowe, N.C. Probing magnetic interactions in metal-organic frameworks and coordination polymers microscopically. *Dalton Trans.* **2018**, *47*, 13257–13280. [[CrossRef](#)] [[PubMed](#)]
5. Gorai, T.; Schmitt, W.; Gunnlaugsson, T. Highlights of the development and application of luminescent lanthanide based coordination polymers, MOFs and functional nanomaterials. *Dalton Trans.* **2021**, *50*, 770–784. [[CrossRef](#)] [[PubMed](#)]
6. Decadt, R.; Van Hecke, K.; Depla, D.; Leus, K.; Weinberger, D.; Van Driessche, I.; Van Der Voort, P.; Van Deun, R. Synthesis, crystal structures, and luminescence properties of carboxylate based rare-earth coordination polymers. *Inorg. Chem.* **2012**, *51*, 11623–11634. [[CrossRef](#)] [[PubMed](#)]
7. Hirai, Y.; Nakanishi, T.; Kitagawa, Y.; Fushimi, K.; Seki, T.; Ito, H.; Hasegawa, Y. Triboluminescence of lanthanide coordination polymers with face-to-face arranged substituents. *Angew. Chem. Int. Ed.* **2017**, *56*, 7171–7175. [[CrossRef](#)]
8. Du, P.-Y.; Li, H.; Fu, X.; Gu, W.; Liu, X. A 1D anionic lanthanide coordination polymer as an adsorbent material for the selective uptake of cationic dyes from aqueous solutions. *Dalton Trans.* **2015**, *44*, 13752–13759. [[CrossRef](#)]
9. Zeng, H.-H.; Qiu, W.-B.; Zhang, L.; Liang, R.-P.; Qiu, J.-D. Lanthanide coordination polymer nanoparticles as an excellent artificial peroxidase for hydrogen peroxide detection. *Anal. Chem.* **2016**, *88*, 6342–6348. [[CrossRef](#)]
10. Chen, H.-J.; Chen, L.-Q.; Lin, L.-R.; Long, L.-S.; Zheng, L.-S. Doped luminescent lanthanide coordination polymers exhibiting both white-light emission and thermal sensitivity. *Inorg. Chem.* **2021**, *60*, 6986–6990. [[CrossRef](#)]
11. Islam, M.J.; Kitagawa, Y.; Tsurui, M.; Hasegawa, Y. Strong circularly polarized luminescence of mixed lanthanide coordination polymers with control of 4f electronic structures. *Dalton Trans.* **2021**, *50*, 5433–5436. [[CrossRef](#)] [[PubMed](#)]
12. Benmansour, S.; Pérez-Herráez, I.; López-Martínez, G.; Gómez-García, C.J. Solvent-modulated structures in anilato-based 2D coordination polymers. *Polyhedron* **2017**, *135*, 17–25. [[CrossRef](#)]
13. Zheng, Z.; Lu, H.; Wang, Y.; Bao, H.; Li, Z.-J.; Xiao, G.-P.; Lin, J.; Qian, Y.; Wang, J.-Q. Tuning of the network dimensionality and photoluminescent properties in homo- and heteroleptic lanthanide coordination polymers. *Inorg. Chem.* **2021**, *60*, 1359–1366. [[CrossRef](#)] [[PubMed](#)]
14. Benmansour, S.; Gómez-García, C.J.; Hernández-Paredes, A. The complete series of lanthanoid-chloranilato lattices with dimethylsulfoxide: Role of the lanthanoid size on the coordination number and crystal structure. *Crystals* **2022**, *12*, 261. [[CrossRef](#)]
15. Fourcade-Cavillou, F.; Trombe, J.-C. Synthesis and crystal structure of $\text{La}(\text{H}_2\text{O})(\text{C}_2\text{O}_4)_2 \cdot (\text{CN}_3\text{H}_6)$ and of $[\text{Nd}(\text{H}_2\text{O})_2(\text{C}_2\text{O}_4)_4 \cdot (\text{NH}_4)(\text{CN}_3\text{H}_6)]$. *Solid State Sci.* **2002**, *4*, 1199–1208. [[CrossRef](#)]
16. Li, Z.-Y.; Zhai, B.; Li, S.-Z.; Cao, G.-X.; Zhang, F.-Q.; Zhang, X.-F.; Zhang, F.-L.; Zhang, C. Two series of lanthanide coordination polymers with 2-methylenesuccinate: Magnetic refrigerant, slow magnetic relaxation, and luminescence properties. *Cryst. Growth Des.* **2016**, *16*, 4574–4581. [[CrossRef](#)]
17. Legendziewicz, J.; Keller, B.; Turowska-Tyrk, I.; Wojciechowski, W. Synthesis, optical and magnetic properties of homo- and heteronuclear systems and glasses containing them. *New J. Chem.* **1999**, *23*, 1097–1103. [[CrossRef](#)]
18. Huskowska, E.; Glowiak, T.; Legendziewicz, J.; Oremek, G. Luminescence and crystal structure of neodymium and europium squarate hydrates. *J. Alloys Compd.* **1992**, *179*, 13–25. [[CrossRef](#)]
19. Takano, R.; Ishida, T. Polymeric terbium(III) squarate hydrate as a luminescent magnet. *Crystals* **2021**, *11*, 1221. [[CrossRef](#)]

20. Reineke, T.M.; Eddaoudi, M.; Fehr, M.; Kelley, D.; Yaghi, O.M. From condensed lanthanide coordination solids to microporous frameworks having accessible metal sites. *J. Am. Chem. Soc.* **1999**, *121*, 1651–1657. [[CrossRef](#)]
21. Daiguebonne, C.; Gérault, Y.; Guillou, O.; Lecerf, A.; Boubekur, K.; Batail, P.; Kahn, M.; Kahn, O. A new honeycomb-like molecular compound: $\text{Gd}[\text{C}_6\text{H}_3(\text{COO})_3](\text{H}_2\text{O})_3 \cdot 1.5\text{H}_2\text{O}$. *J. Alloys Comp.* **1998**, *275*, 50–53. [[CrossRef](#)]
22. Wang, S.-J.; Tian, Y.-W.; You, L.-X.; Ding, F.; Meert, K.W.; Poelman, D.; Smet, P.F.; Ren, B.-Y.; Sun, Y.-G. Solvent-regulated assemblies of 1D lanthanide coordination polymers with the tricarboxylate ligand. *Dalton Trans.* **2014**, *43*, 3462–3470. [[CrossRef](#)] [[PubMed](#)]
23. Mathis II, S.R.; Golafale, S.T.; Solntsev, K.M.; Ingram, C.W. Anthracene-based lanthanide metal-organic frameworks: Synthesis, structure, photoluminescence, and radioluminescence properties. *Crystals* **2018**, *8*, 53. [[CrossRef](#)]
24. You, L.-X.; Cao, S.-Y.; Guo, Y.; Wang, S.-J.; Xiong, G.; Dragutan, I.; Dragutan, V.; Ding, F.; Sun, Y.-G. Structural insights into new luminescent 2D lanthanide coordination polymers using an $\text{N,N}'$ -disubstituted benzimidazole zwitterion. Influence of the ligand. *Inorg. Chim. Acta* **2021**, *525*, 120441. [[CrossRef](#)]
25. Wu, Y.; Zhou, Y.; Cao, S.; Cen, P.; Zhang, Y.-Q.; Yang, J.; Liu, X. Lanthanide metal—Organic frameworks assembled from unexplored imidazolylcarboxylic acid: Structure and field-induced two-step magnetic relaxation. *Inorg. Chem.* **2020**, *59*, 11930–11934. [[CrossRef](#)] [[PubMed](#)]
26. Wang, Z.-X.; Wu, Q.-F.; Liu, H.-J.; Shao, M.; Xiao, H.-P.; Li, M.-X. 2D and 3D lanthanide coordination polymers constructed from benzimidazole-5,6-dicarboxylic acid and sulfate bridged secondary building units. *CrystEngComm* **2010**, *12*, 1139–1146. [[CrossRef](#)]
27. Chen, Y.; Zhao, X.; Gao, R.; Ruan, Z.; Lin, J.; Liu, S.; Tian, Z.; Chen, X. Temperature-induced solvent assisted single-crystal-to-single-crystal transformation of $\text{Mg}(\text{II})$ - $\text{Ln}(\text{III})$ heterometallic coordination polymers. *J. Solid State Chem.* **2020**, *292*, 121674. [[CrossRef](#)]
28. García-García, A.; Zabala-Lekuona, A.; Goñi-Cárdenas, A.; Cepeda, J.; Seco, J.M.; Salinas-Castillo, A.; Choquesillo-Lazarte, D.; Rodríguez-Diéguez, A. Magnetic and luminescent properties of isostructural 2D coordination polymers based on 2-pyrimidinecarboxylate and lanthanide ions. *Crystals* **2020**, *10*, 571. [[CrossRef](#)]
29. Abhervé, A.; Mañas-Valero, S.; Clemente-León, M.; Coronado, E. Graphene related magnetic materials: Micromechanical exfoliation of 2D layered magnets based on bimetallic anilate complexes with inserted $[\text{Fe}^{\text{III}}(\text{acac}_2\text{-trien})]^+$ and $[\text{Fe}^{\text{III}}(\text{sal}_2\text{-trien})]^+$ molecules. *Chem. Sci.* **2015**, *6*, 4665–4673. [[CrossRef](#)]
30. Ashoka Sahadevan, S.; Abhervé, A.; Monni, N.; Sáenz de Pipaón, C.; Galán-Mascarós, J.R.; Waerenborgh, J.C.; Vieira, B.J.C.; Auban-Senzier, P.; Pillet, S.; Bendeif, E.; et al. Conducting anilate-based mixed-valence $\text{Fe}(\text{II})\text{Fe}(\text{III})$ coordination polymer: Small-polaron hopping model for oxalate-type $\text{Fe}(\text{II})\text{Fe}(\text{III})$ 2D networks. *J. Am. Chem. Soc.* **2018**, *140*, 12611–12621. [[CrossRef](#)]
31. Benmansour, S.; Gómez-García, C.J. Lanthanoid-anilate complexes and lattices. *Magnetochemistry* **2020**, *6*, 71. [[CrossRef](#)]
32. Ashoka Sahadevan, S.; Monni, N.; Abhervé, A.; Marongiu, D.; Sarritzu, V.; Sestu, N.; Saba, M.; Mura, A.; Bongiovanni, G.; Cannas, C.; et al. Nanosheets of two-dimensional neutral coordination polymers based on near-infrared-emitting lanthanides and a chlorocyananilate ligand. *Chem. Mater.* **2018**, *30*, 6575–6586. [[CrossRef](#)]
33. Benmansour, S.; Hernández-Paredes, A.; Bayona-Andrés, M.; Gómez-García, C.J. Slow relaxation of the magnetization in anilate-based $\text{Dy}(\text{III})$ 2D lattices. *Molecules* **2021**, *26*, 1190. [[CrossRef](#)] [[PubMed](#)]
34. Abrahams, B.F.; Hudson, T.A.; McCormick, L.J.; Robson, R. Coordination polymers of 2,5-dihydroxybenzoquinone and chloranilic acid with the (10,3)-*a* topology. *Cryst. Growth Des.* **2011**, *11*, 2717–2720. [[CrossRef](#)]
35. Darago, L.E.; Aubrey, M.L.; Yu, C.J.; Gonzales, M.I.; Long, J.R. Electronic conductivity, ferrimagnetic ordering, and reductive insertion mediated by organic mixed-valence in a ferric semiquinoid metal-organic framework. *J. Am. Chem. Soc.* **2015**, *137*, 15703–15711. [[CrossRef](#)] [[PubMed](#)]
36. Monni, N.; Andres-Garcia, E.; Caamaño, K.; García-López, V.; Clemente-Juan, J.M.; Giménez-Marqués, M.; Oggianu, M.; Cadoni, E.; Mínguez Espallargas, G.; Clemente-León, M.; et al. A thermally/chemically robust and easily regenerable anilate-based ultramicroporous 3D MOF for CO_2 uptake and separation. *J. Mater. Chem. A* **2021**, *9*, 25189–25195. [[CrossRef](#)]
37. Abrahams, B.F.; Coleiro, J.; Ha, K.; Hoskins, B.F.; Orchard, S.D.; Robson, R. Dihydroxybenzoquinone and chloranilic acid derivatives of rare earth metals. *J. Chem. Soc. Dalton Trans.* **2002**, *8*, 1586–1594. [[CrossRef](#)]
38. Bondaruk, K.; Hua, C. Effect of counterions on the formation and structures of $\text{Ce}(\text{III})$ and $\text{Er}(\text{III})$ chloranilate frameworks. *Cryst. Growth Des.* **2019**, *19*, 3338–3347. [[CrossRef](#)]
39. Wang, Y.; Liu, X.; Li, X.; Zhai, F.; Yan, S.; Liu, N.; Chai, Z.; Xu, Y.; Ouyang, X.; Wang, S. Direct radiation detection by a semiconductive metal-organic framework. *J. Am. Chem. Soc.* **2019**, *141*, 8030–8034. [[CrossRef](#)]
40. Ashoka Sahadevan, S.; Monni, N.; Abhervé, A.; Cosquer, G.; Oggianu, M.; Ennas, G.; Yamashita, M.; Avarvari, N.; Mercuri, M.L. Dysprosium chlorocyananilate-based 2D-layered coordination polymers. *Inorg. Chem.* **2019**, *58*, 13988–13998. [[CrossRef](#)]
41. Huang, G.; Yang, P.; Wang, N.; Wu, J.-Z.; Yu, Y. First lanthanide coordination polymers with N,N -dimethylformamide hydrolysis induced formate ligands. *Inorg. Chim. Acta* **2012**, *384*, 333–339. [[CrossRef](#)]
42. Seidel, C.; Lorbeer, C.; Cybińska, J.; Mudring, A.-V.; Ruschewitz, U. Lanthanide coordination polymers with tetrafluoroterephthalate as a bridging ligand: Thermal and optical properties. *Inorg. Chem.* **2012**, *51*, 4679–4688. [[CrossRef](#)] [[PubMed](#)]
43. Chen, B.; Yang, Y.; Zapata, F.; Qian, G.; Luo, Y.; Zhang, J.; Lobkovsky, E.B. Enhanced near-infrared-luminescence in an erbium tetrafluoroterephthalate framework. *Inorg. Chem.* **2006**, *45*, 8882–8886. [[CrossRef](#)] [[PubMed](#)]

44. Ashoka Sahadevan, S.; Monni, N.; Oggianu, M.; Abhervé, A.; Marongiu, D.; Saba, M.; Mura, A.; Bongiovanni, G.; Mameli, V.; Cannas, C.; et al. Heteroleptic NIR-emitting YbIII/Anilate-based neutral coordination polymer nanosheets for solvent sensing. *ACS Appl. Nano Mater.* **2020**, *3*, 94–104. [[CrossRef](#)]
45. Ashoka Sahadevan, S.; Manna, F.; Abhervé, A.; Oggianu, M.; Monni, N.; Mameli, V.; Marongiu, D.; Quochi, F.; Gendron, F.; Le Guennic, B.; et al. Combined experimental/theoretical study on the luminescent properties of homoleptic/heteroleptic erbium(III) anilate-based 2D coordination polymers. *Inorg. Chem.* **2021**, *60*, 17765–17774. [[CrossRef](#)]
46. Atzori, M.; Artizzu, F.; Marchiò, L.; Loche, D.; Caneschi, A.; Serpe, A.; Deplano, P.; Avarvari, N.; Mercuri, M.L. Switching-on luminescence in anilate-based molecular materials. *Dalton Trans.* **2015**, *44*, 15786–15802. [[CrossRef](#)]
47. Llunell, M.; Casanova, D.; Girera, J.; Alemany, P.; Alvarez, S. *SHAPE*; Version 2.1; Universitat de Barcelona: Barcelona, Spain, 2010.
48. Artizzu, F.; Deplano, P.; Marchiò, L.; Mercuri, M.L.; Pilia, L.; Serpe, A.; Quochi, F.; Orrù, R.; Cordella, F.; Saba, M.; et al. New insights on infrared emitters based on er-quinolinolate complexes: Synthesis, characterization, structural and photophysical properties. *Adv. Funct. Mater.* **2007**, *17*, 2365–2376. [[CrossRef](#)]